A Generalized Pressure Load Model for Anti-Slosh Baffles at Different Fill Depths and Slosh Wave Heights

H. Q. Yang[1], Marco D. Sansone, Jacob M. Brodnick, and Brandon R. Williams[3]
[1]CFD Research Corp., Huntsville, Alabama, USA
[2]Amentum, Huntsville, Alabama, USA
[3]NASA Marshall Space Flight Center, Alabama, USA

Propellant sloshing can significantly affect both spacecraft stability and the structural integrity of propellant tanks. Anti-slosh baffles are commonly employed to mitigate these effects, with their configuration typically guided by damping requirements. Accurate knowledge of distributed pressure loading is essential for baffle structural design, while the resulting forces and moments are directly relevant to vehicle control system design. Previous experimental studies on rigid ring baffles have characterized liquid pressure loads and associated damping. These studies showed that when the nondimensional velocity parameter exceeds 3.0, the previous theoretical predictions agree with measurements; however, at values below 3.0, existing theories become nonconservative and underpredict pressure loads. In this work, a generalized pressure load model is derived from the principle of energy conservation. Computational fluid dynamics (CFD) simulations indicate that slosh-induced pressure can be decomposed into static and transient components, and that a phase shift in pressure occurs across the baffle, increasing with fluid damping. The maximum load corresponds to a 90° phase shift. Comparisons with comprehensive experimental data validate the proposed theory, showing that when the baffle is submerged, the maximum pressure load model encompasses all measured data. The theory is further extended to predict pressure loads at varying fill depths and wave heights, demonstrating very good agreement with experimental results. The simple mathematical model derived in this study provides a robust predictive tool for pressure loading across different fill depths and slosh wave heights, supporting both structural and control system design.

I. INTRODUCTION

Propellant slosh is a major disturbance source that influences the dynamic stability of space vehicles. The fluid motion is typically represented by a spring–mass–damper mechanical analog incorporated into the vehicle's equations of motion for guidance, navigation, and control (GNC) analysis. This representation requires parameters such as the natural frequency of the dominant slosh mode, the effective slosh mass, its center of motion, and the critical damping ratio. During the 1960s U.S. space program, these parameters were estimated through analytical solutions for simple geometries or obtained from sub-scale experiments. Subsequent studies by the authors [1] demonstrated that a CFD-based approach can accurately capture detailed tank-sloshing behavior and extract equivalent mechanical parameters over a wide range of configurations and fill levels.

---

[1] Chief Scientist, Aerospace and Defense Solutions, CFD Research Corporation, 6820 Moquin Dr. NW, Huntsville, AL, 35806, USA, AIAA Associate Fellow.
[2]Amentum, Huntsville, Alabama, USA
[3] Fluid Dynamics Branch-ER42, George C. Marshall Space Flight Center, AL 35812, AIAA Member

Validation studies [1] compared CFD predictions for cylindrical tanks against analytical solutions and sub-scale Centaur LOX/LH_2 tanks (both with and without baffles) showing excellent agreement for natural frequency, slosh mass, and center-of-mass location. These results confirm that CFD can reliably provide mechanical properties for arbitrary tank geometries, which is especially valuable for the design of new tanks where experimental data are limited.

Slosh forces can strongly couple with vehicle structures or control systems when the oscillation frequency of the liquid coincides with either the vehicle's fundamental elastic-bending mode or the dynamic control frequency during powered flight. Such coupling may lead to excessive vibrations or trajectory deviation [2]. Therefore, sufficient damping of the liquid motion must be considered in performance and stability analyses.

Baffles of various geometries are commonly used to enhance damping and reduce slosh-induced forces and torques [2]. However, minimizing launch-vehicle mass often favors lightweight tanks with fewer or thinner baffles, creating challenges in maintaining structural integrity under distributed pressure loading. Accurate prediction of this loading is essential for baffle design, while the resulting net forces and moments are critical inputs to control-system analysis.

Earlier researchers addressed the baffle-pressure problem using analytical or semi-theoretical formulations. Liu [4] proposed an analytical method based on irrotational sloshing, whereas Davis [5] introduced a semi-empirical expression that incorporates both fluid acceleration and velocity effects. The NASA monograph Propellant Slosh Loads [6] summarized maximum-pressure correlations for submerged baffles based on the experiments of Keulegan and Carpenter [7]. More comprehensive testing by Scholl et al. [5] measured pressure distributions and damping coefficients for rigid ring baffles over a wide range of fill depths and oscillation periods. Figure 1 shows that existing theories reproduce the data well for nondimensional velocity parameters above 3.0, but significantly underpredict pressure loads between 0.5 and 3.0—especially when the baffle is partially exposed.

The objective of this paper is to develop a generalized pressure load model that aligns with experimental data across varying baffle depths and wave heights. A theory for the maximum possible pressure on a baffle is first derived, yielding a maximum pressure of $\sqrt{2}\,\rho g\eta$, where η is the slosh wave height. The model is then extended to predict pressures at different wave heights and fill levels, providing a robust tool for structural and control system design.

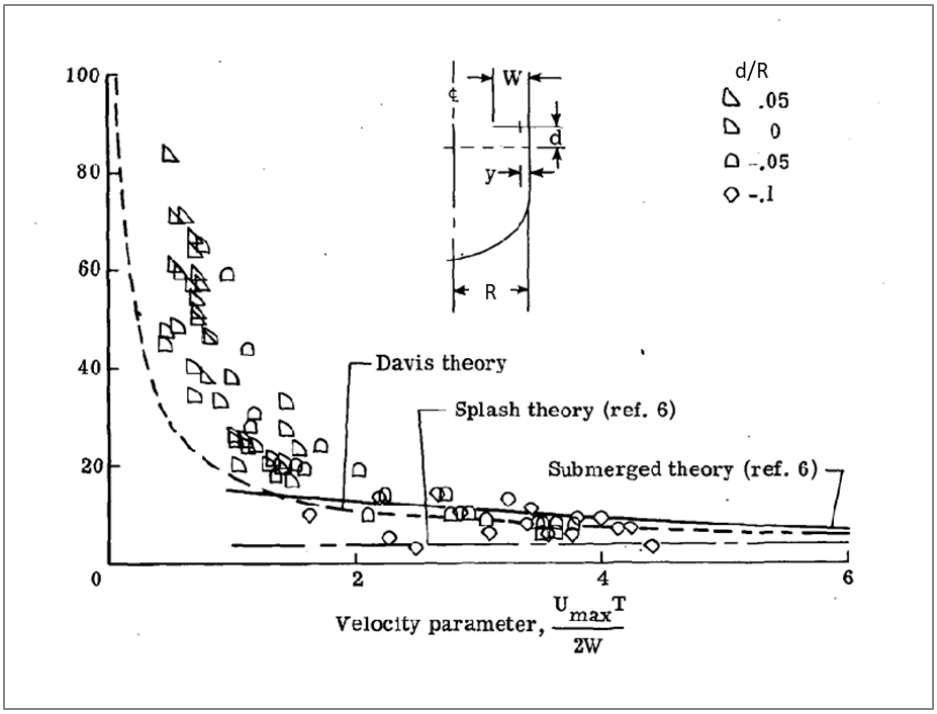

Figure 1. Previous development of the theoretical model on nondimensional pressure with nondimensional velocity parameter [5]

II. PROCESS

The following describes the derivation of the proposed maximum slosh pressure load theory. The basis of this theory will subsequently be verified using high-fidelity CFD simulations.

2.1 Development of Slosh Pressure Load Theory

Slosh motion can be represented by a spring–mass–damper model in which energy is periodically exchanged between potential and kinetic components. During one oscillation cycle, the liquid alternately stores potential energy in the displaced free surface and kinetic energy in the bulk motion of the fluid. The potential energy is $\rho g \eta$, and the kinetic energy is formed from the mass of the slosh mass and its velocity. See Figure 2 for the definition of wave height η.

Based on Bernoulli's principle:

$$\frac{\rho v^2}{2} + \rho g h + p = constant \tag{1}$$

The maximum oscillatory gauge pressure amplitude—occurring when the wave crest reaches its peak and the local velocity is zero is given by the hydrostatic pressure

$$p_\eta = \rho g \eta \tag{2}$$

At any location within the tank, the instantaneous pressure may be written as the sum of a static component (no slosh) and a transient component induced by slosh motion:

$$p = p_{static} + p_{transient} \tag{3}$$

The hydrostatic pressure at maximum potential energy is equivalent to transient pressure at maximum kinetic energy as the wave returns to a minimal potential energy. Because the global slosh motion can be represented by a sinusoidal function, the transient term becomes

$$p_{transient} = p_\eta \sin(\omega t + \theta); \text{ with: } \max(p_\eta) = \rho g \eta \tag{4}$$

Neglecting static-pressure variation across the baffle, the dynamic pressure difference from Eq. (4) is

$$\Delta p = p_\eta \, sin(\omega t + \theta_1) - p_\eta \, sin(\omega t + \theta_2) = \rho g \eta [sin(\omega t + \theta_1) - sin(\omega t + \theta_2)] \tag{5}$$

where θ_1 is the phase angle at the top of the baffle relative to the free surface wave. θ_2 is the phase angle at the bottom of the baffle relative to the free surface wave. The phase shift between the top and bottom of the baffle $(\theta_1 - \theta_2)$ is due to damping in the fluid. The maximum of Eq. (5) occurs at a phase shift of 90 degrees, yielding the highest pressure load:

$$\max(\Delta p_\eta) = \max(\rho g \eta [sin(\omega t + \pi/2) - sin(\omega t)]) = p_\eta [\sin(\omega t + \theta_1) - \sin(\omega t + \theta_2)] = \sqrt{2} \rho g \eta \tag{6}$$

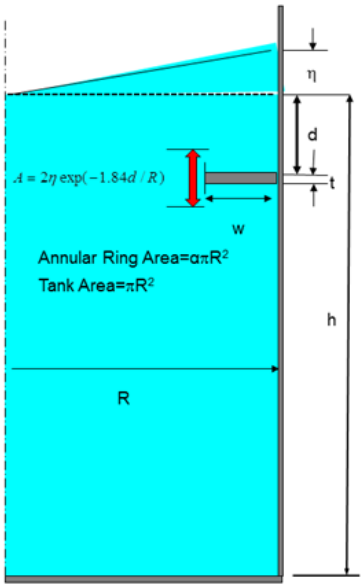

Figure 2. Definition of related quantities for a submerged baffle. h: liquid fill level; η: wave height; d: baffle depth from the free surface; R: liquid tank radius; w: baffle width.

2.2 CFD Verification of The Maximum Slosh Pressure Load Theory

A CFD model has been built to verify the proposed pressure load theory. The model is shown in Figure 3, and it has the following parameters:

- Cylindrical tank with tank radius, R = 165"
- The liquid fill level from tank bottom, h = 2R; baffle width (W): 12”
- Liquid: LH2; density: 70.8 kg/m^3
- Initial wave height: η = 4”
- Baffle depth, d: d/R = 0.0, 0.05, 0.1, 0.25
- Total number of cells: 0.5 million
- Pressure monitor points from tank wall: 0.25W, 0.5W, 0.75W

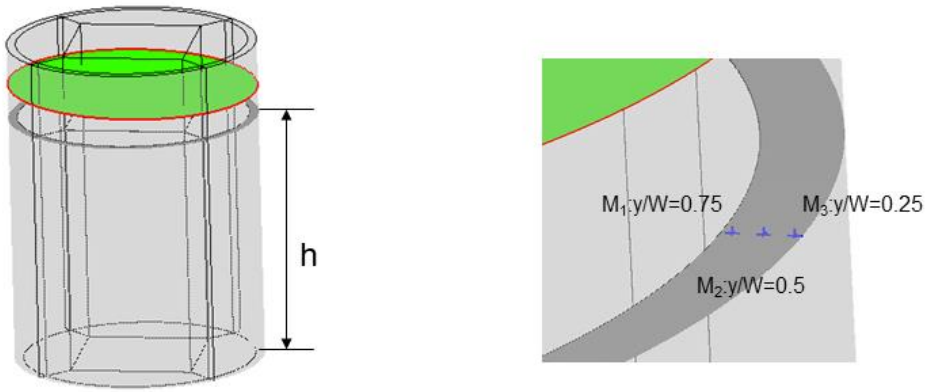

Figure 3. CFD model used to verify the maximum pressure load theory. The green surface is the fluid and gas interface with the red line showing the intersection with the tank wall. The anti-slosh baffle is submerged below the interface.

Verification #1: Max Local Transient Pressure Magnitude is $\rho g \eta$

Restating Eq. (3) and Eq. (4), the pressure field is decomposed into static and transient components:

$$p = p_{static} + p_{transient} \tag{7}$$

$$p_{transient} = p_\eta \sin(\omega t + \theta); \text{ with: } \max(p_\eta) = \rho g \eta \tag{8}$$

The maximum transient amplitude is $\rho g \eta$, and η is the initial wave height. Figure 4 presents the CFD-predicted transient pressure at the mid-width location (y/W=0.5) for points above and below the baffle, as well as their differential, for the three depths (d/R=0.25, d/R=0.1, and d/R=0.0). Pressures are normalized by the theoretical maximum from Eq. (8) using an initial wave height of 4" ($\rho g \eta$).

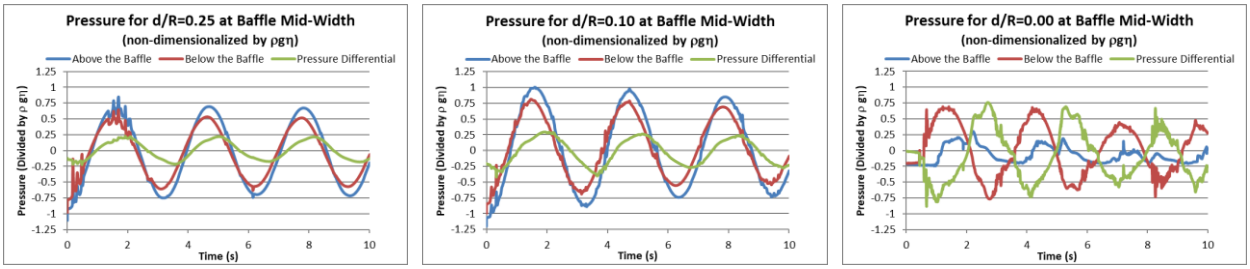

Figure 4. Nondimensional transient pressure around baffles at different depth ratios (d/R) from the free surface at the mid-width location (y/W=0.5)

The results confirm that the pressure oscillates periodically at the slosh frequency, $f = \frac{1}{2\pi}\sqrt{\frac{1.84g}{R}} = 0.330$ Hz [2]. The hydrostatic component $\rho g h$, has been subtracted, leaving only the transient contribution. The amplitude of this component is always less than unity in nondimensional form, verifying that the local transient pressure magnitude is bounded by $\rho g \eta$.

Verification #2: There is a Phase Shift in Pressure Across the Baffle

We propose that the pressure load is:

$$p_{top} = p_\eta \sin(\omega t + \theta_1) \tag{9}$$

$$p_{bottom} = p_\eta \sin(\omega t + \theta_2) \tag{10}$$

Figure 4 shows a clear phase shift across the baffle that increases as the fill level decreases. For d/R=0.25, $(\theta_1 - \theta_2) = 6.95\ deg.$; for d/R=0.10, $(\theta_1 - \theta_2) = 8.76\ deg.$; and for d/R=0.0, $(\theta_1 - \theta_2) = 88.4\ deg.$ The phase shift is a result of damping inside the fluid. A larger phase shift implies a higher damping. The largest phase shift occurs at d/R=0.0 and is close to 90 degrees.

Verification #3: Max Pressure Load is $\sqrt{2}\rho g\eta$

We assume that the pressure phase differs across the baffle.

$$\Delta p = p_\eta[sin(\omega t + \theta_1) - sin(\omega t + \theta_2)] \tag{11}$$

Let us assume that the phase shift has a maximum value of $(\theta_1 - \theta_2) = 90\ deg.$

Use the following expression:

$$\begin{aligned} \Delta p &= p_\eta[sin(\omega t + \theta_1 + 90^o) - sin(\omega t + \theta_1)] \\ &= p_\eta[cos(\omega t + \theta_1) - sin(\omega t + \theta_1)] \\ &= \sqrt{2} p_\eta\, sin(\omega t + \theta_1 - 45^o) = \sqrt{2}\rho g\eta\, sin(\omega t + \theta_1 - 45^o) \end{aligned} \tag{12}$$

This arrives at our maximum load of $\sqrt{2}\rho g\eta$. Figure 4 includes the pressure differential across the baffle non-dimensionalized by the maximum transient pressure $\rho g\eta$. Based on the above derivation, the maximum non-dimensional pressure across the baffle should be less than $\sqrt{2}$. Figure 4 shows that for both baffle depths of d/R=0.25 and d/R=0.10, the nondimensional values are around 0.25. For the depth ratio of d/R=0.0, the nondimensional value is larger at about 0.75. But the maximum is less than our derivation of 1.41.

Figure 5 shows the transient pressures at the baffle root. The results again verify that none of the computed pressure loads across the baffle are higher than $\sqrt{2}\rho g\eta$ ($\sqrt{2}$ in the nondimensional form) at different fill levels.

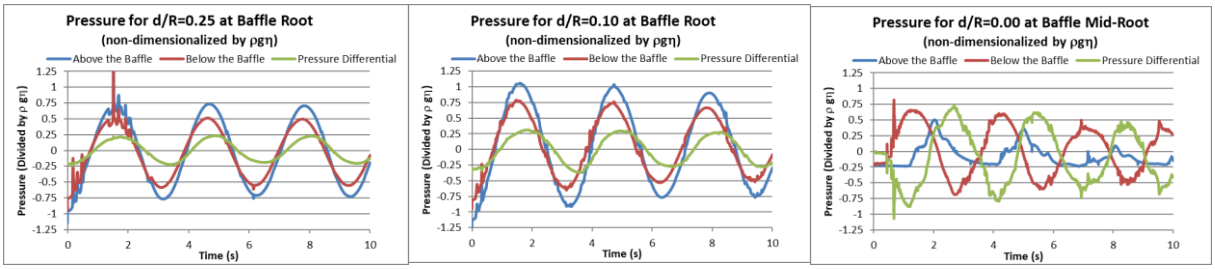

Figure 5. Nondimensional transient pressure load on baffle root (y/W=0.25) at different depth ratios (d/R) from the free surface.

2.3 Validation of Slosh Pressure Load Theory

An extensive investigation by Scholl et al. [5] examined the pressure loads and damping associated with rigid ring baffles in large cylindrical tanks (Figure 6). Their study measured the radial and circumferential pressure distribution and damping coefficients on a ring baffle excited by the fundamental antisymmetric slosh mode in a 284-cm-diameter tank. Experimental and analytical data were reported as functions of slosh velocity or amplitude, baffle spacing, and baffle location above or below the free surface.

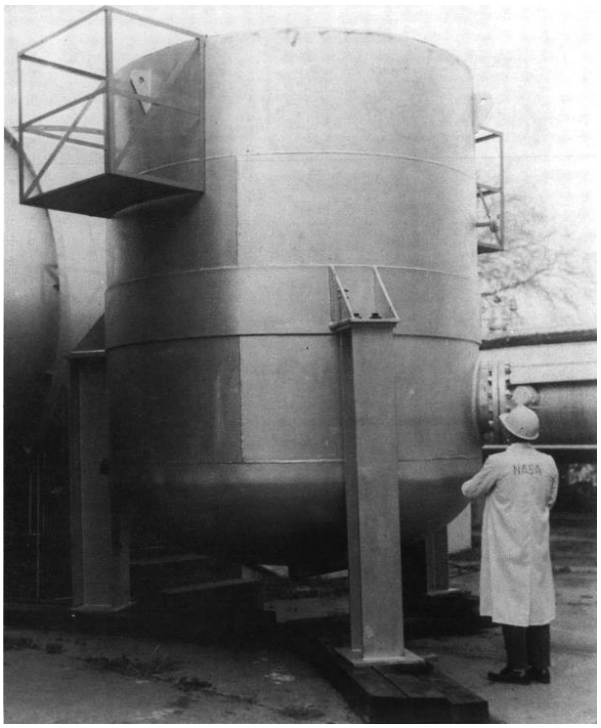

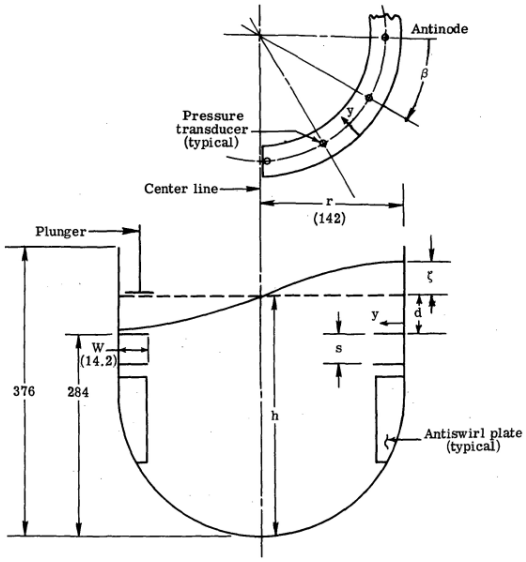

Test condition	d/r	s/W	y/W	β, deg
Single baffle	-0.1 to +0.4		0.25, 0.5, and 0.75	0 to 90
Two baffles	0 to 0.4	0.5 to 2.0	0.5	0

Figure 6. Slosh tank with 284cm diameter (left); tank and baffle variables [5].

The measured pressure data are presented in terms of a reduced velocity parameter. $\frac{U_{max}T}{2W}$, which is a nondimensional parameter (often referred to as the period parameter) describing the relative velocity. Here U_{max} is the maximum liquid velocity at the baffle location; T is the natural period of the oscillation, and W is the baffle width. The maximum vertical velocity in a cylindrical tank at the baffle location due to the antisymmetric mode may be written as [5]:

$$U_{max} = \omega\eta_{max} sinh\left(1.84\frac{h-d}{R}\right)/sinh\left(1.84\frac{h}{R}\right) \tag{13}$$

where ω is the natural slosh frequency, η_{max} is the maximum displacement amplitude of the surface, d is the distance of the baffle below the quiescent surface, R is the tank radius, and h is the liquid depth. When the baffle is located at or below the quiescent surface, the value obtained from Eq. (13) at the baffle depth may be used to obtain the value of the reduced velocity parameter.

In the presentation of experimental work and previous analytical results [5], the pressure is non-dimensionalized as:

$$\bar{p} = \frac{P}{\frac{1}{2}\rho {U_{max}}^2} \tag{14}$$

Let us define: $U_{max} = \omega\eta$, where $\omega = 2\pi f;\ f$: slosh frequency, T: slosh period, and $T = \frac{1}{f}$. Combining with the predicted maximum pressure load from Eq. (6), we have:

$$\frac{p_{max}}{\frac{1}{2}\rho {U_{max}}^2} = \frac{1.41\rho g\eta}{\frac{1}{2}\rho(\omega\eta)^2} = \frac{2.82g}{\omega^2\eta} \tag{15}$$

For a straight cylinder with a neglected bottom effect, one has [2]:

$$\omega^2 = \frac{1.84g}{R}, \qquad \text{and} \quad \frac{U_{max}T}{2W} = \frac{\pi\eta}{W} \tag{16}$$

Now, our nondimensional maximum pressure load will be:

$$\bar{p}_{max} = \frac{p_{max}}{\frac{1}{2}\rho {U_{max}}^2} = \frac{4.81}{\left(\frac{U_{max}T}{2W}\right)}\left(\frac{R}{W}\right) \quad (17)$$

It should be emphasized that the nondimensional baffle pressure load is not only a function of the nondimensional velocity parameter but also a function of the baffle width-to-tank radius ratio.

Validation of Maximum Pressure Theory

Figure 7 presents the experimental data (black symbols), previous theories (black lines), current CFD simulations (red symbols), and our maximum pressure theory (blue line) based on the derived Equation (17), evaluated at the baffle quarter-width location of y/W=0.25. The results include experimental cases for baffle depth ratios of d/R=-0.05, 0, 0.05, 0.1, 0.2, 0.3, and 0.4.

For the fully submerged cases (d/R >0.1), Davis' theory agrees well with experimental data at velocity parameters greater than 1.0. However, at velocity parameters below 1.0, Davis' theory underpredicts the pressure load. Similarly, the submerged theory also underestimates the pressure in this low-velocity regime.

Our CFD results are consistent with the experimental findings of Scholl et al. [5], as the predictions fall within the experimental scatter, thereby validating the accuracy of our simulations. Importantly, the proposed maximum pressure theory provides a conservative prediction, generally enveloping the experimental data across the range of conditions examined.

Figure 8 shows the experimental data (black symbols), previous theories (black lines), the current CFD simulation results (red symbols), and our maximum pressure theory (blue line) at the midpoint of the baffle (y/W=0.50) for the case when the interface is close to the baffle. Results for different baffle depths are plotted together. As observed, Davis' theory aligns reasonably well with experimental data when the velocity parameter exceeds 2.0. However, for lower velocity parameters (<2.0), significant discrepancies exist between the theory and experimental measurements. The same is true for the submerged theory. The CFD simulations fall within the range of experimental data [5]. Notably, our maximum pressure theory (Eq. 17) substantially improves upon Davis' predictions and successfully envelopes all submerged baffle depths.

Figure 8 shows that, in some cases where d/R < 0—corresponding to the settled free surface being below the baffle—the experimental pressures exceed the predictions of the maximum pressure theory. When the liquid fill level is close to the baffle (small d/R) and the wave height exceeds the baffle depth (η/R > d/R), the liquid can splash onto the baffle. Such splashing not only enhances slosh damping but can also generate short-duration, high-pressure pulses that surpass the proposed maximum pressure. CFD simulations capture these dynamics, revealing that splash-induced collision pressures are highly localized and occur on time scales much shorter than a slosh period.

For load characterization, slosh loads and splash loads should be treated as distinct phenomena because they transfer energy to the baffle structure through different mechanisms. Slosh loads act periodically at low frequencies, exciting low-order structural modes with limited damping and thus enabling sustained oscillations. In contrast, splash loads are impulsive, excite higher-order modes (which are more strongly damped), and occur at much lower frequencies. As a result, splashes rarely excite resonant high-order modes that could cause unbounded amplitude growth, making them less critical for baffle design than slosh loads.

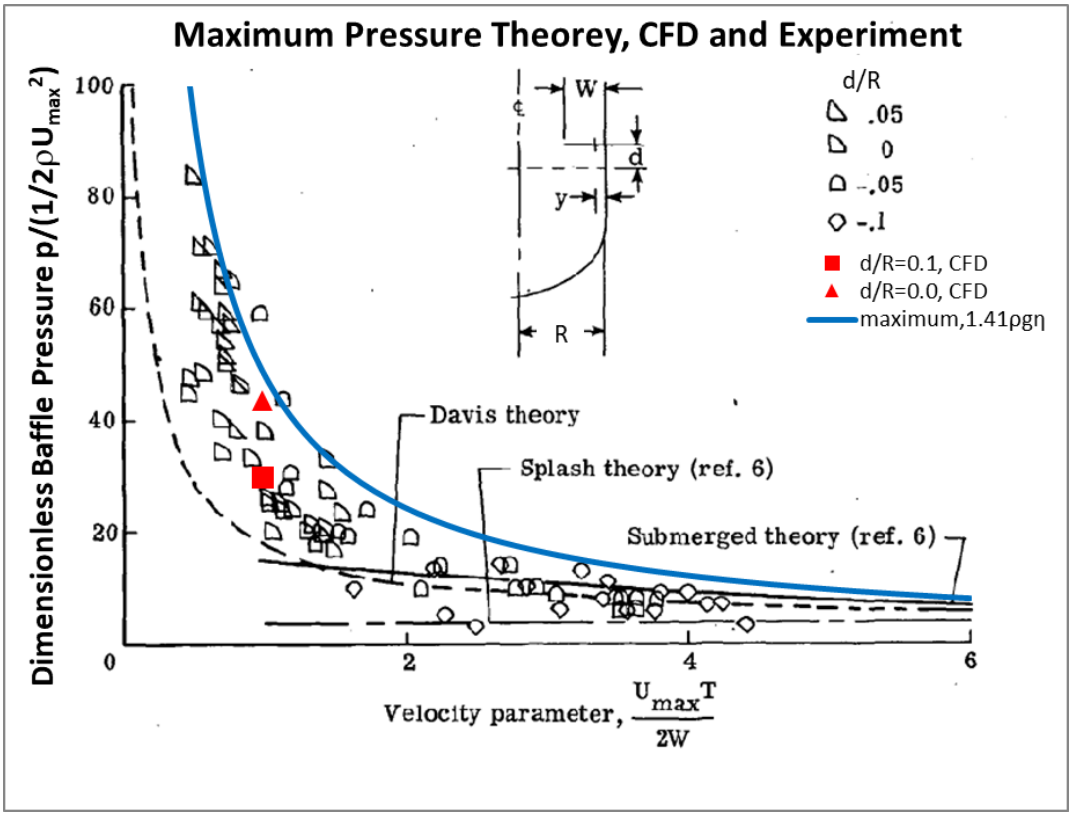

(a) Submerged baffle

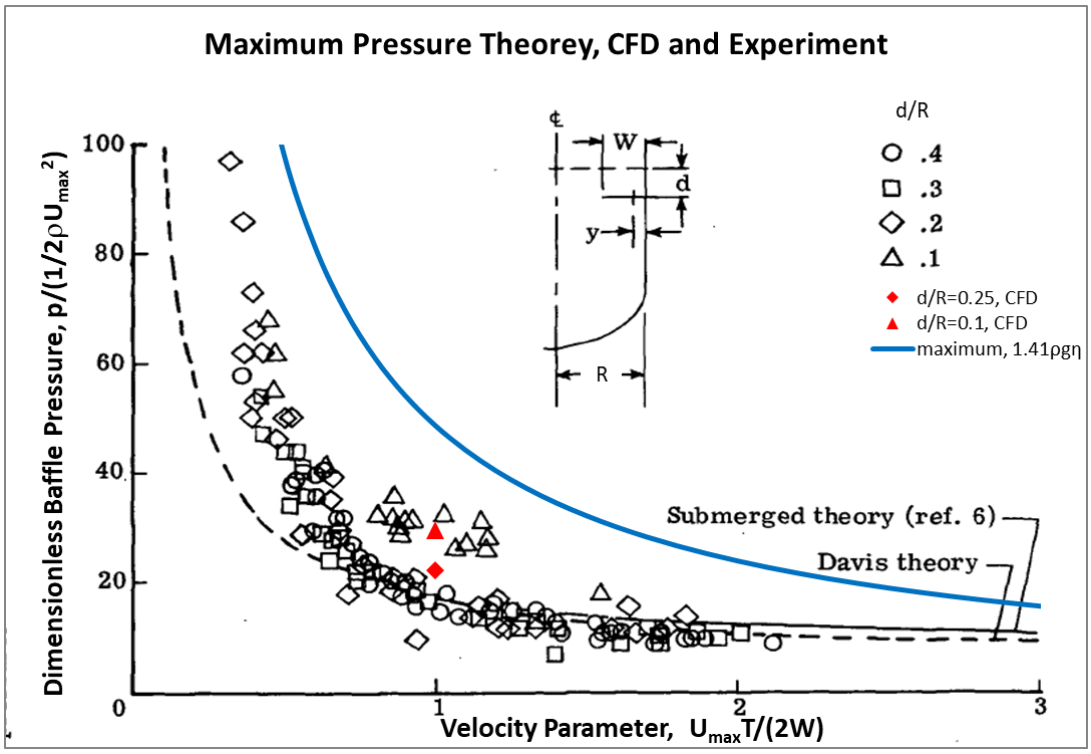

(b) Baffle near the free surface.

Figure 7. Nondimensional pressure comparison at baffle quarter width ($y/W = 0.25$) between experimental data, previous theories, CFD, and the current maximum pressure theory for low d/R

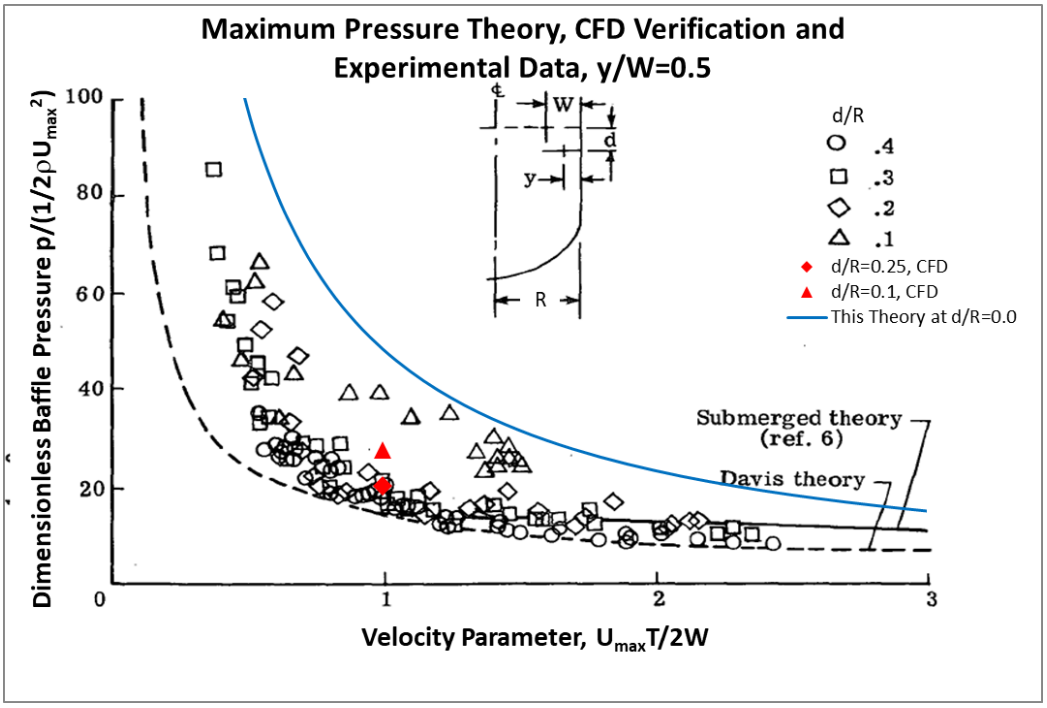

(a) Submerged baffle

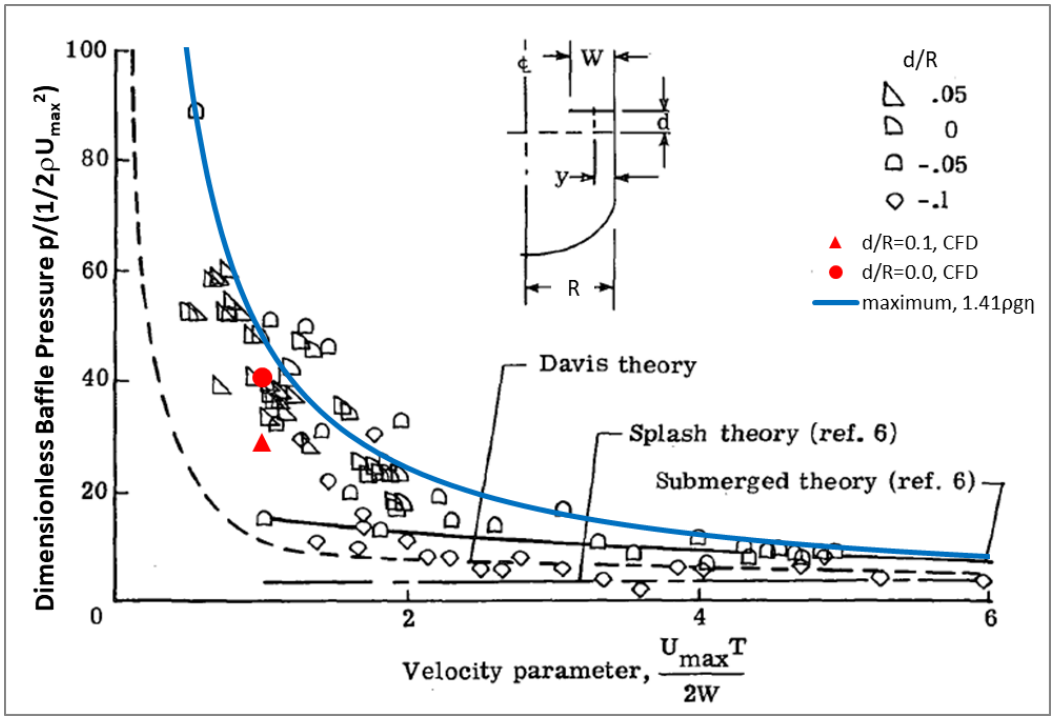

(b) Baffle near the free surface

Figure 8. Pressure comparison at the mid of the baffle ($y/W = 0.50$) between experimental data, previous theories, CFD, and the current maximum pressure theory (Equation 17)

Figure 9 further illustrates that even in the presence of splashing, slosh loads predominantly remain bounded by the proposed maximum pressure theory, supporting its applicability at fill levels very near the baffle. However, because experimental data at these fill levels likely contain both slosh and splash contributions—and the data analysis methodology is not fully documented—it is not possible to definitively confirm the contribution of splash loads to the reported pressures.

Finally, Figure 10 compares the present theory with experimental data at the baffle tip (y/W=0.75). The CFD predictions again agree closely with the measurements, and the proposed maximum pressure theory ($\sqrt{2}\rho g\eta$) provides a conservative envelope for the observed pressures.

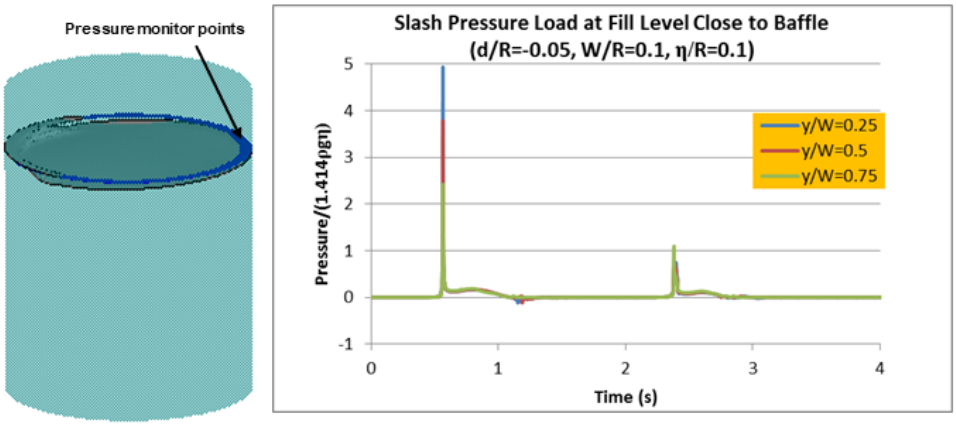

Figure 9. Computed high-pressure spike due to splash during slosh when the baffle is slightly above the free surface.

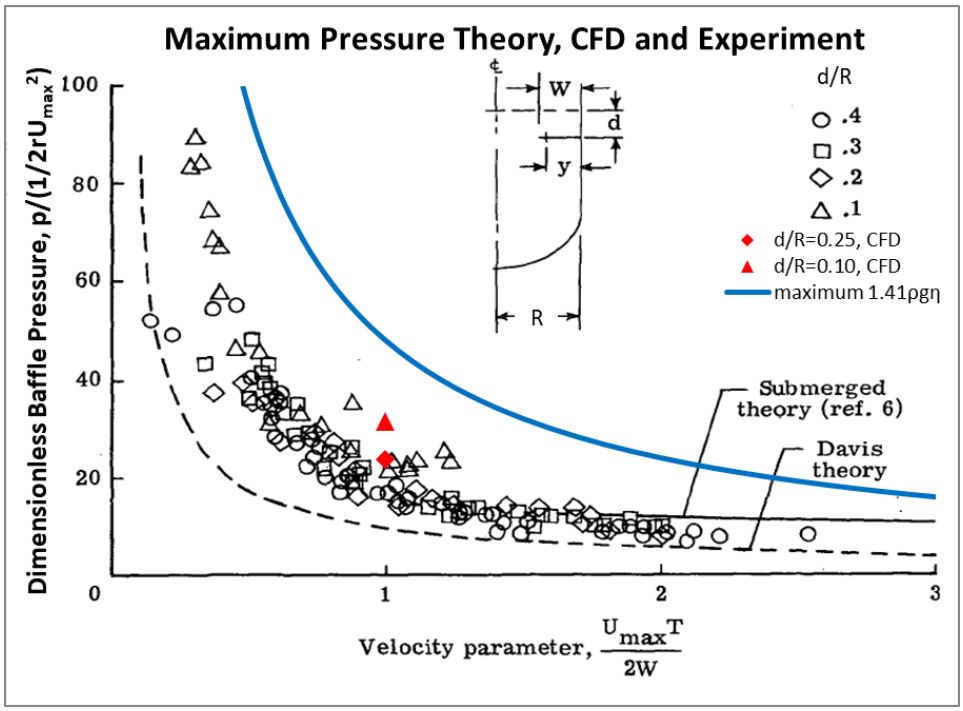

Figure 10. Pressure comparison at the tip of the baffle ($y/W = 0.75$) between experimental data, previous theories, CFD, and the current maximum pressure theory

2.4 Derivation and Validation of Slosh Pressure Load at Different Fille Levels.

Our maximum pressure load represents the maximum value of the pressure load, which typically occurs when the baffle is near the liquid interface. In the practical design, it is desirable to have an accurate representation of the above model for different fill depths and different wave heights. Based on the potential solution of the slosh equation, the amplitude of flow particle movement at different fill levels can be written as [3]

$$\eta_d = \eta \exp\left(-\frac{1.84d}{R}\right) \tag{18}$$

Our generalized pressure model can then be expressed as:

$$p_d = \sqrt{2}\rho g \eta * \exp\left(-\frac{1.84d}{R}\right) \tag{19}$$

Figure 11 shows the comparison of experimental data, CFD prediction, and theoretical models of dimensionless baffle pressure at the baffle midpoint (y/W=0.5). Experimental measurements are shown as black symbols for various baffle depths (from d/r=0.1 to 0.4), CFD predictions as red solid symbols, the proposed maximum pressure theory as blue symbols and lines, and existing theories (Davis and submerged [6]) as dashed black lines. From the plot, one can see that the proposed depth dependence of slosh pressure load is consistent with the experimental trend: the highest pressure is at zero depth, and the pressure decreases with the fill level depth. As the theoretical plot has the same symbol style, the theoretical models indeed envelop the experimental measurement.

The experimental data at other baffle locations of y/W=0.25 and y/W=0.75, in addition to the mid point of y/W=0.5, are compared to the proposed theoretical model Eq. (19) in Figure 12 for d/R=0.1 at (a), d/R=0.2 at (b), d/R=0.3 at (c), and d/R=0.4 at (d). It is clear that the proposed maximum pressure theory (Eq. 19) envelopes all the submerged cases **(**d/r>0) and provides a conservative bound for design.

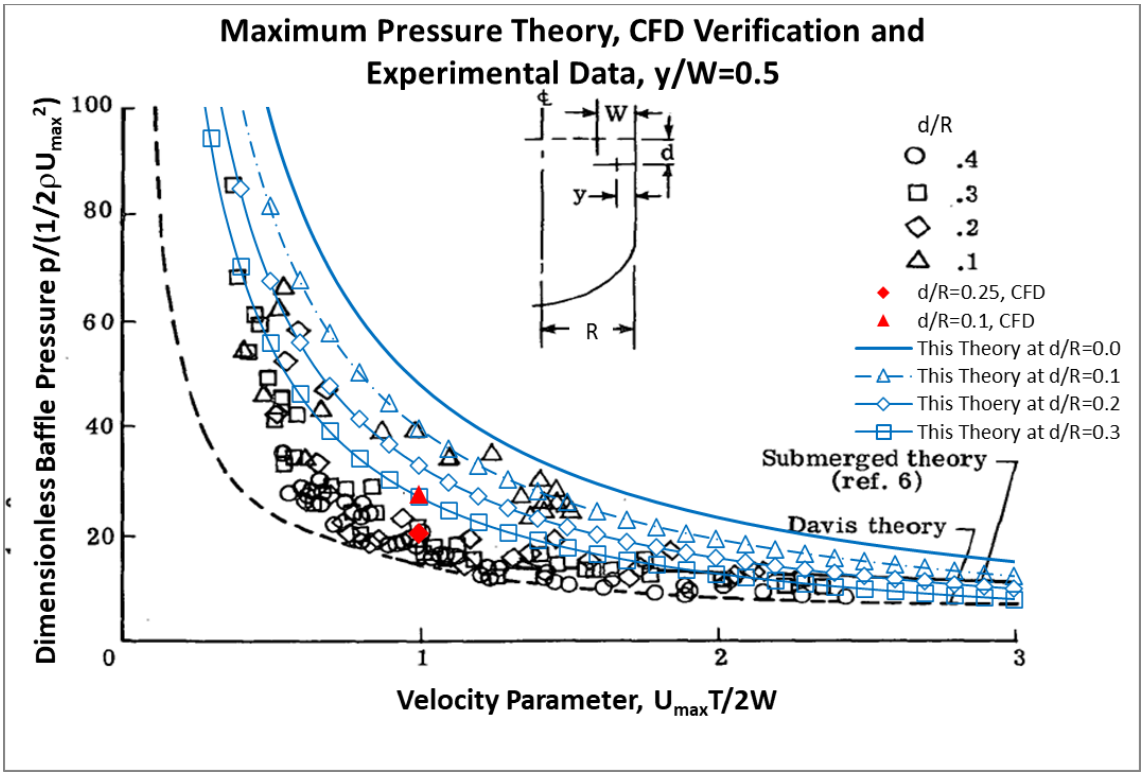

Figure 11. Comparison of experimental data, CFD predictions, and theoretical models of dimensionless baffle pressure at the baffle midpoint (y/W=0.5)

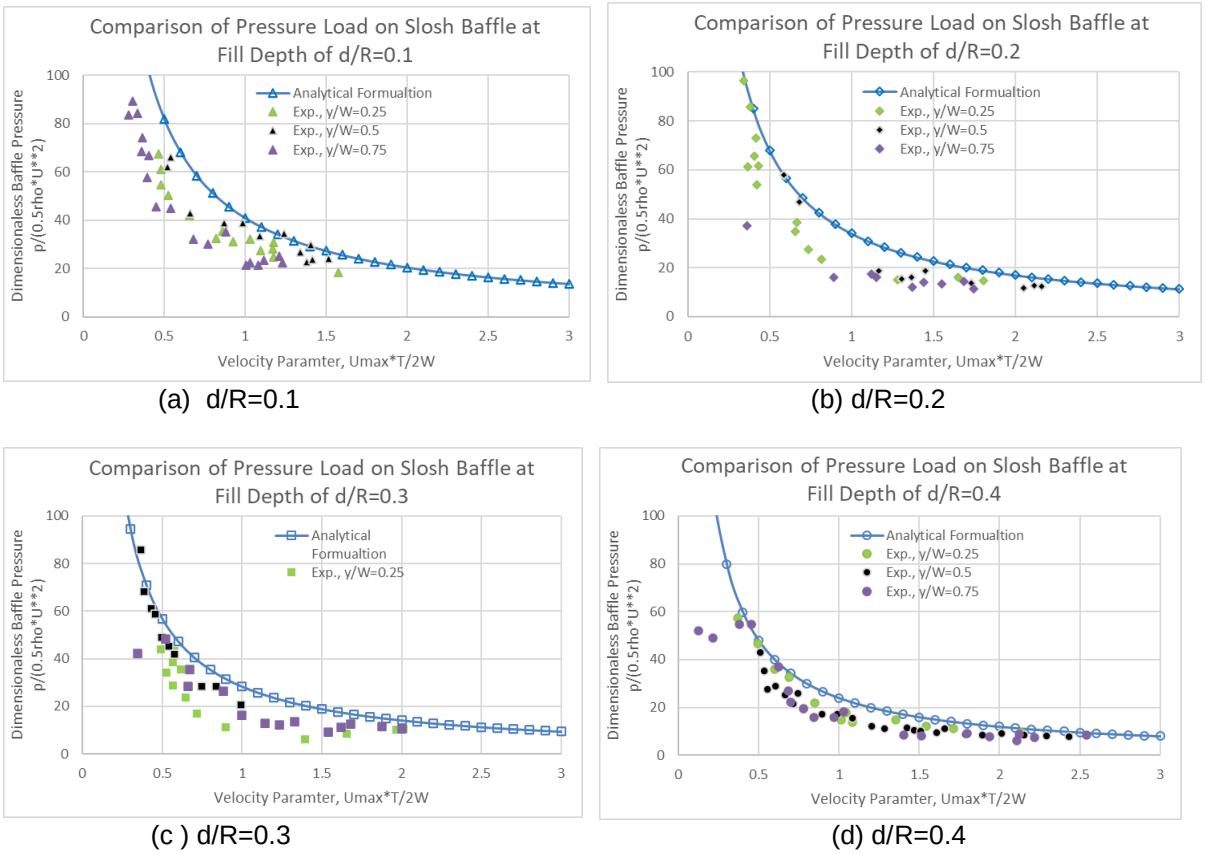

Figure 12. Comparison of the generalized pressure load model with experimental data at different liquid depths.

III. SUMMARY AND CONCLUSIONS

A generalized analytical model has been developed to predict the distributed pressure loads on ring-type anti-slosh baffles under various fill depths and slosh amplitudes. The model is based on an energy-conservation argument that leads to a maximum dynamic pressure corresponding to a 90° phase shift across the baffle. Moreover, the model's closed-form analytical expression allows straightforward application in design calculations, offering both accuracy and simplicity.

CFD results confirm the theoretical assumptions and highlight the gradual transition from slosh-dominated to splash-dominated regimes as the free surface impacts the baffle. When the wave crest strikes the underside of the baffle, short-duration pressure spikes—referred to as splash loads—occur. These transient peaks are not periodic and result from localized jetting and entrapped gas compression. While splash loads may exceed the mean maximum slosh pressure, their occurrence is highly intermittent and spatially localized. Therefore, in engineering design practice, they are typically addressed through local safety factors or transient structural analysis rather than slosh-like periodic load models.

Key findings are summarized as follows:

1. The maximum local transient pressure magnitude is bounded by $\rho g \eta$, consistent with both theory and CFD results.
2. The phase shift across the baffle increases with decreasing liquid depth, reaching 90∘ degrees for a fully exposed baffle.
3. The theoretical maximum pressure $p_{max} = \sqrt{2}\rho g \eta$ provides a conservative upper limit that envelopes all experimental data.

4. The generalized model incorporating depth variation accurately predicts the decrease in pressure with increasing submergence.
5. The model remains valid for submerged configurations and provides a unified framework for estimating baffle pressure loads in both design and control-system analyses.

In conclusion, the present study unifies theoretical, numerical, and experimental insights into a simple predictive model suitable for engineering design. The derived maximum-pressure-load expression can be readily implemented in design codes to assess baffle strength and support sizing. Future work will focus on extending the model to include compressibility and free-surface impact phenomena associated with splash loading and partial vacuum formation.

Acknowledgments

This study was performed by a Task Order of Amentum, NASA MSFC ESSCA Contract 80MSFC18C0011. Dr. Ram Ramachandran was the Amentum ESSCA Task Lead.

REFERENCES

1. H. Q. Yang and J. W. Peugeot, Propellant Sloshing Parameter Extraction from CFD Analysis, *Journal of Spacecraft and Rockets*, Vol. 51, No. 3 (2014), pp. 908-916.
2. H. N. Abramson, "The Dynamic Behavior of Liquids in Moving Containers," NASA SP-106, 1967.
3. J. W. Miles, "On the Sloshing of Liquid in a Cylindrical Tank. Report. No. AM6-5, Gal-TR-18, The Ramo-Wooldridge Corp., Guided Missile Research Div., Apr. 1956.
4. Liu, F.C., "Pressure On Baffle Rings Due To Fuel Sloshing In A Cylindrical Tank," NASA-MSFC Aero-Astrodynamics Internal Note 4-64, January 1964.
5. Scholl, H.F., Stephens, D.G., Davis, P.K., "Ring-Baffle Pressure Distribution and Slosh Damping In Large Cylindrical Tanks," NASA TN D-6870 (1972).
6. Braslow, A. L., "Propellant Slosh Loads," NASA Space Vehicle Design Criteria (Structures), NASA SP-8009, 1968.
7. Keulegan, G.H., Carpenter, L.H., "Forces On Cylinders And Plates In An Oscillating Fluid," Journal of Research of the National Bureau of Standards (1958).
8. Miles, J.W., "Ring Damping Of Free Surface Oscillations In A Circular Tank," Journal of Applied Mechanics (1958).